Evaluating the Effectiveness of Brain Tumor Image Generation using Generative Adversarial Network with Adam Optimizer

Aryaf Al-Adwan
Department of Autonomous Systems, Al-Balqa Applied University, Al-Salt, Jordan

***Abstract*—Deep learning models known as Generative Adversarial Networks (GANs) have shown great potential in several applications, such as computer vision and image synthesis. They are now a viable tool in medical imaging, useful for tasks like improving diagnostic model performance, generating new images, and augmenting existing data. This paper aims to utilize the capabilities of GANs to produce synthetic MRI images, with the purpose of enhancing the training dataset for tumor classification. A new method is presented to classify tumors in MRI images by combining GANs and Convolutional Neural Networks (CNNs). This method employed the Adam optimizer and the Binary Cross Entropy (BCE) with Logits Loss as the criterion, where they contributed in optimizing the training process and stabilizing the GANs. The proposed method in this paper achieved an average accuracy of 95.1% and an average loss of 0.080 with large images. Furthermore, the proposed method is evaluated based on Peak Signal-to-Noise Ratio (PSNR) and Structural Similarity Index (SSIM) and is compared to the existing models of GAN. These outcomes highlight the potential of the GAN-based approach in contributing to improved medical diagnostics and treatments.**

Keywords*—Generative Adversarial Networks; images; medical; Convolutional Neural Networks

I. INTRODUCTION

Medical image data is paramount in modern healthcare, playing a pivotal role in enabling accurate diagnoses, precise treatment planning, and effective disease monitoring. However, the development and evaluation of robust machine-learning algorithms for medical imaging face significant hurdles due to limited data availability and concerns regarding patient privacy. Increasing reliance on medical imaging modalities like MRI, CT, and ultrasound has generated big imaging data. Overcoming these challenges necessitates innovative approaches to advance medical imaging analysis and ultimately enhance patient outcomes [1].

Convolutional Neural Networks (CNNs) are a form of deep learning models that have demonstrated significant promise in diverse fields. They has been effectively implemented in a variety of computer vision applications, including object detection, classification, and image denoising. CNN is a modified form of a feed-forward neural network, where the neurons in the early layers perform convolution operations. The CNN architecture consists of two stages: a feature extractor and a classifier. In combination, they enable autonomous feature extraction and end-to-end training, with minimal pre-processing requirements [2-3].

GANs have emerged as a transformative tool with the potential to address critical issues surrounding data availability, patient privacy, and data diversity. GANs comprise generator and discriminator networks engaged in an adversarial learning process. By harnessing this framework, GANs can learn the underlying distribution of real medical images and generate synthetic counterparts that exhibit remarkable realism and fidelity. This remarkable capability provides promising solutions to the scarcity of annotated medical data by facilitating the generation of large volumes of labeled images. These synthetic images, created through GANs, become invaluable resources for training deep learning models across various tasks, including classification, segmentation, and detection [4].

GAN-generated images are instrumental in addressing data imbalance and the limited availability of datasets representing rare medical conditions. By augmenting limited datasets, GAN-generated images enhance the effectiveness of medical image analysis algorithms, allowing for more comprehensive and robust evaluations. Moreover, GANs offer privacy-preserving data-sharing mechanisms by anonymizing sensitive patient information within synthetic images [5-6]. This unique attribute enables large-scale multi-center studies and strengthens the generalizability of models by facilitating data exchange and collaboration while upholding patient privacy. Synthetic medical images generated by GANs also serve as valuable resources for data augmen-tation, effectively mitigating overfitting and enhancing the overall performance and reliability of medical image analysis algorithms [7].

Evaluating GANs using quantitative measures and classification performance is important for several reasons. Firstly, it allows us to assess the quality and fidelity of the synthetic medical images generated by GANs. Quantitative measures such as Mean Squared Error (MSE), PSNR and SSIM, [8], provide objective metrics to evaluate the similarity between GAN-generated images and real images from the original dataset. These measures help us understand the extent to which GANs successfully capture the characteristics and details of the original medical images [9-10]. In addition, classifica-tion performance evaluation using deep learning models trained on GAN-generated images provides insights into the utility and practicality of these synthetic images. By comparing the performance metrics such as accuracy, recall, and F1 score of the mod-els trained on GAN-generated images with those trained on the original dataset, we can determine the suitability of GAN-generated images for downstream tasks

such as diagnosis or disease classification. This analysis sheds light on the effectiveness of GAN-generated images as viable substitutes or supplements to real medical images [11-12].

By achieving these research objectives and evaluating GANs using quantitative measures and classification performance, we can contribute to understanding the strengths, limitations, and potential applications of GANs in generating synthetic medical images. Therefore, this research has practical implications in healthcare, such as improving the availability and diversity of medical image datasets, enhancing pri-vacy protection, and facilitating the development of accurate and robust medical im-age analysis and diagnosis models [13-14].

It is worth to mention that the proposed method is a GAN-based approach which can produce synthetic MRI images that closely resemble the actual ones. The GAN will be trained using a broad dataset, which included tumor and no-tumor images of various sizes, in order to accurately capture the characteristics and variances inherent in the original dataset. The GAN's ability to generate high-quality and realistic images will be evident from the evaluation metrics, such as PSNR, MSE, and SSIM, which indicate a close resemblance between the generated and original images. Also the choice of Adam optimizer will have the impact on the training process, due to the powerful of the optimizer in affecting the important factors that play important role in the training process of neural networks within the GAN.

The research objectives of this paper are twofold: Firstly, to evaluate GANs in the context of generating synthetic medical images, and secondly, to assess the effectiveness of the enhanced version of GAN-generated images through quantitative measures and classification performance. Furthermore, the proposed method is evaluated based on Peak Signal-to-Noise Ratio (PSNR) and Structural Similarity Index (SSIM) and is compared to the existing models of GAN. These outcomes highlight the potential of the GAN-based approach in contributing to improved medical diagnostics and treatments.

II. Related Works

The literature on GANs for medical image generation and evaluation has witnessed significant growth, reflecting the increasing interest in leveraging GANs to ad-dress challenges in the medical imaging domain. This section provides an overview of the relevant literature, highlighting critical studies and approaches in this field.

Authors in study [15] proposed a conditional generative adversarial network (cGAN) for synthesizing COVID-19 CT images. The method addresses data scarcity and infection risks by generating realistic CT images. The cGAN demonstrates superior performance in image quality metrics and shows potential for machine learning applications. The synthesized images can be used for data augmentation, training of intern radiologists, and transferability to other medical imaging domains. Future research uses synthetic images for specific computer vision approaches in COVID-19 diagnosis.

Compared the performance of a GAN and a residual network (ResNet) for generating synthetic CT images from MR images for radiation therapy planning. The ResNet model exhibits superior accuracy in delineating brain tissues compared to the GAN model. Both models show relative structural similarity and peak signal-to-noise ratio values, but the ResNet model generates less noisy and more similar synthetic CT images. This research suggests the potential of the ResNet model for accurate synthetic CT generation in MRI-only radiation therapy planning and PET/MR attenuation correction [16].

Authors in study [17] introduced a deep learning methodology using a GAN to improve the image quality and computed tomography (CT) number accuracy of daily cone beam CT (CBCT). The algorithm called 2.5 Pix2pix GAN with feature matching (FM) outperforms other methods regarding image quality, reducing artifact distortion and improving soft tissue contrast. The generated synthetic CT (sCT) images demonstrate high accuracy compared to reference CT (rCT) images, and the dosimetry calculation accuracy is also evaluated, showing promising results for photon-based planning. The proposed algorithm is computationally efficient and has the potential to support online CBCT-based adaptive radiotherapy.

An approach that was focusing on generating synthetic contrast-enhanced CT (sCECT) images from non-contrast chest CT (NCCT) images using a deep learning model was proposed in [18]. The sCECT images exhibit higher image similarity metrics and improved contrast-to-noise ratio of mediastinal lymph nodes compared to NCCT images. Radiologists detect more lymph nodes and rate higher lesion conspicuity on NCCT with sCECT compared to NCCT alone. The findings highlight the technical feasibility of using deep learning to generate sCECT images from NCCT, providing additional diagnostic information. However, it is emphasized that synthetic images should not replace contrast-enhanced CT but complement it in specific clinical scenarios.

Authors in study [19] presented a two-stage GAN approach for data augmentation in image segmentation tasks, specifically focusing on cell nuclei image segmentation. The proposed approach generated synthesized binary masks and incorporates them to generate corresponding synthesized images. The generated image-mask pairs enhance the performance of conventional image segmentation models. Extensive evaluations on a benchmark cell nuclei image segmentation dataset demonstrate the proposed approach’s superiority over traditional and existing GAN-based augmentation methods. This approach shows promise for improving image segmentation in medical imaging with limited annotated data.

An approach that was focusing evaluating the use of Deep Convolutional Generative Adversarial Networks (DCGAN) for data augmentation of chest X-ray images. USING A LIMITED DATASET, the DCGAN generates synthetic chest X-ray images representing the under-represented class (Normal). Evaluation using the Fréchet Distance of Inception (FID) score indicates a close resemblance between the generated and original images. A neural network classifier trained on the DCGAN augmented dataset performs better than traditional augmentation methods. DCGAN-based data augmentation offers a practical approach to improving classifier performance in medical image analysis tasks [20].

The authors in study [21] collected and analyzed 105 papers on medical image augmentation, highlighting the organs represented in the images, datasets used, loss functions employed, and evaluation metrics utilized. The paper summarized the advantages of different augmentation models, loss functions, and evaluation metrics, providing valuable insights for researchers designing augmentation tasks. It also explored the relationship between augmented models and the training set size, emphasizing the role of augmentation in scenarios with limited training data quality. The review indicated the strong development momentum in this research field and discusses existing limitations and potential research directions. GAN-based medical image augmentation is an effective approach to address the challenge of limited training samples in medical image diagnosis and treatment models.

Another research investigated the effectiveness of GANs in synthesizing high-resolution pathology images of ten cancer histological types [22]. Board-certified pathologists and pathology trainees evaluate the quality of the synthetic images. The results show that the synthetic images are classified by histotype with comparable accuracy to real images and are visually indistinguishable from them. Deep convolution-al neural networks trained on the synthetic images perform as well as those trained on additional real images when diagnosing different cancer types. The findings have important applications in proficiency testing, quality assurance, and training computer aided diagnostic systems. Synthetic images, such as rare cancers, can also be valuable when labeled datasets are limited. A publicly available website is provided for clinicians and researchers to participate in an image survey related to this research.

A supervised 3D GAN framework [29] to accurately predict CT images based on MRI data where a contextual information is integrated into the GAN framework for medical image synthesis was introduced in [23]. In addition, a unique loss is introduced to mitigate the problem of blurriness in the obtained CT. The research results clearly illustrate that the suggested approach exhibits good performance to the compared techniques.

The Adaptive Moment Estimation (AME) algorithm, or Adam optimizer, which was utilized to optimize the training of deep neural networks, such as RNN, CNN, and GANs was presented in [24]. It helps with the modification of the learning rate and accelerates convergence and bias correction by automatically modifying the parameters. Moreover, it divides the parameter updates by the square root of the second moment to normalize the parameter. This helps to stabilize the optimization process and lessen the effects of large gradients, resulting in training that is more resilient and trustworthy.

Authors in study [25] introduced the Least Squares Generative Adversarial Networks (LSGAN), which is a modified version of a regular GAN that used the least squares for the training of the generator and the discriminator. Therefore, instead of discrete binary outputs, the least squares yielded continuous valued outputs that neared the intended labels and provided smoother gradients. On the other hand, another form of GANs, known as InfoGAN, was presented in [26]. It seeks to create different and controllable samples of a generated image by changing specific latent features. This resulted in latent codes that could be utilized to control and change particular attributes of the generated samples. Nonetheless, training InfoGAN requires careful consideration of hyperparameters, such as the trade-off between adversarial loss and mutual information regularization.

Wasserstein Generative Adversarial Networks (WGAN) was introduced in by the authors in study [27] as another variant of GAN. One of the fundamental ideas of WGAN is to guarantee the Wasserstein distance is well-defined and calculable by applying a Lipschitz constraint on the discriminator network.

WGAN guarantees that the discriminator's gradients with respect to its inputs are restricted by limiting the discriminator's Lipschitz constant, which improves the discriminator's convergence properties and produces safer training.

Some of these papers mentioned earlier demonstrated the growing interest in leveraging GANs for medical image generation and evaluation across various medical imaging tasks. The results highlight the potential of GANs to generate realistic medical images, enhance image quality, and improve the performance of diagnostic and segmentation models. Additionally, the studies emphasize the value of synthetic images in addressing challenges such as limited data, data scarcity, and the need for data augmentation. The findings contribute to the advancement of GAN-based approaches in the medical imaging domain and suggest future research directions further to explore the capabilities of GANs in medical image analysis.

III. METHODOLOGY

The methodology section of this paper involves data collection and preprocessing for brain tumor classification as the following subsections.

A. Dataset (MRI)

The dataset used is BRAIN TUMOR MRI DATASET, which is a combination of three datasets: figshare, SARTAJ dataset, and Br35H. It contains 7023 human brain MRI images, classified into four classes: glioma, meningioma, no tumor and pituitary as shown in Fig. 1. The "no tumor" class images were sourced from the Br35H dataset. However, there is an issue with the glioma class images in the SARTAJ dataset, as they are not categorized correctly. This observation was made based on the results of other studies and models trained using the dataset. To address this problem, the glioma images from the SARTAJ dataset were removed, and the images from the figshare site were used instead. The images in the dataset have different sizes. As part of the pre-processing step, we plan to resize the images to the desired size after removing extra margins. This preprocessing step is expected to improve the accuracy of the model.

B. Data Preprocessing

In the data preprocessing step, the collected MRI images undergo several transformations to ensure they are suitable for the subsequent classification task. The following preprocessing steps are applied:

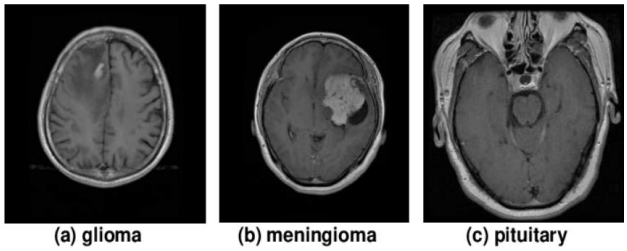

Fig. 1. Sample of the brain tumor MRI dataset for the classes: (a) glioma, (b) meningioma, (c) pituitary, [28].

- Image Resizing: Since the original MRI images have different sizes, resizing them to a uniform size is necessary. Resizing the images to a consistent dimension will facilitate training and ensure compatibility with the chosen classification model.
- Margin Removal: The preprocessed images may contain extra margins or borders that do not contribute to the tumor classification. These margins are removed to focus solely on the relevant regions of the brain containing the tumors. Removing unnecessary margins helps improve the accuracy of the classification model.

C. Proposed Method

The proposed method consists of three main steps: firstly, utilizing a GAN to generate MRI images. Secondly, evaluating the image quality using metrics such as PSNR, MSI and SSIM. Thirdly, performing tumor classification on the generated dataset to observe any differences compared to the original dataset.

The general structure of a GAN is shown in Fig. 2, which consists of a generator and a discriminator network. The generator network, implemented in the Generator class, takes a random noise vector as input and generates synthetic MRI images. It uses a sequence of transposed convolutional layers with batch normalization and ReLU activation to up sample and refine the features. The output of the generator is a synthetic MRI image. The discriminator network, implemented in the Discriminator class, takes an MRI image (real or synthetic) as input and predicts the probability of the image being real. It uses a sequence of convolutional layers with spectral normalization and LeakyReLU activation to extract features and make the classification. The output of the Discriminator is the probability value.

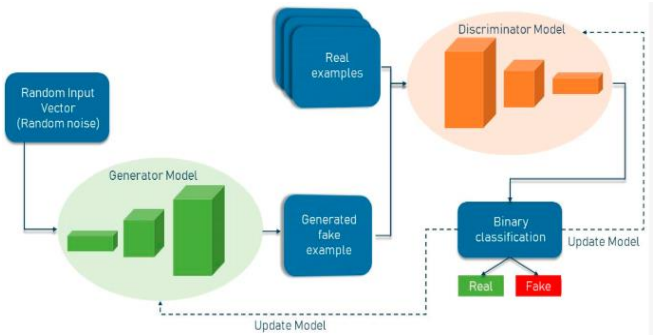

Fig. 2. General Structure of Generative Adversarial Network.

The training process, implemented in the train_GAN function, involves optimizing the Generator and Discriminator networks using an adversarial training scheme. The discriminator is trained to distinguish between real and fake images, while the Generator is trained to generate realistic images that can fool the Discriminator. This process is iterated for multiple epochs, with both networks updated using the Adam optimizer and the binary cross entropy with Logits Loss as the criterion. The progress is printed during training, displaying the current epoch, batch, and loss values for both the discriminator and Generator networks. Additionally, every 10th batch, the Generator generates a set of synthetic images, and a selected number of these images are saved to the specified directory.

To use this proposed method, the train_GAN function is called twice: once for training on the normal MRI images and once for training on the tumor MRI images. The input directories and the desired number of generated images can be customized accordingly.

The following are the main parts of the proposed method:

1) GAN for MRI image generation: The methodology involves training a GAN to generate synthetic MRI images. The generator network learns to generate visually realistic MRI images that resemble real images through an adversarial training process. On the other hand, the discriminator network aims to classify the origin of the images correctly. The GAN training process involves alternating between training the Generator and the discriminator networks, updating their weights based on loss functions specific to each network.

Table I presents the GAN network architecture for MRI image generation. This architecture can be customized and expanded based on the specific requirements of the task. The generator network inputs a random latent vector and generates synthetic MRI images. The discriminator network, on the other hand, takes an MRI image as input and predicts whether it is real or synthetic. Additional layers, such as convolution-al, dense, and reshaped, were incorporated to capture finer details and spatial dependencies in the generated images. It is important to note that hyperparameters tuning, Adam optimizer, cross entropy and regularization techniques played a significant role in training GANs effectively.

TABLE I. GAN NETWORK ARCHITECTURE FOR MRI IMAGE GENERATION

Component	Details
Generator Network (G)	Input: Random latent vector
	Dense layer: Maps the latent vector to a higher-dimensional space
	Reshape layer: Reshapes the output of the dense layer to a 3D volume
	Convolutional layers: Upsample and refine features
	Output: Synthetic MRI image
Discriminator Network (D)	Input: MRI image (real or synthetic)
	Convolutional layers: Extract features
	Flatten layer: Flattens the output of convolutional layers
	Dense layers: Perform classification based on extracted features
	Output: Probability of the input image is real

The generator network takes a random latent vector as input, a random seed for generating synthetic MRI images. This latent vector is processed through a dense layer, mapping it to a higher-dimensional space. The output of the dense layer is then re-shaped into a 3D volume corresponding to the desired size of the MRI image. Convolutional layers upsample and refine features, capturing intricate patterns and details. The final output of the generator network is a visually realistic synthetic MRI image.

Conversely, the discriminator network takes an MRI image as input, which can be either a real image from the dataset or a synthetic image generated by the generator network. The input image is processed through convolutional layers to extract relevant features, capturing important patterns and structures. These features are then flattened and fed into dense layers for classification. The discriminator network evaluates the likelihood of the input image being real or synthetic, producing a probability score as output.

The generator and discriminator networks are trained alternately through an adversarial training process. This iterative training process helps refine the Generator's ability to produce high quality and visually realistic MRI images. The performance of the GAN network relies on factors such as hyperparameter tuning, optimization algorithms, and regularization techniques, which were carefully selected and optimized to ensure effective training and generation of MRI images.

2) Evaluation metrics: After generating the synthetic MRI images using the GAN, the next step is to evaluate the quality of these generated images. Three commonly used evaluation metrics are mentioned: PSNR, MSI and SSIM.

PSNR measures the difference between the generated and original images based on signal noise, while MSI assesses the structural similarity between the two sets of images. These metrics provide quantitative measures of the fidelity and similarity between the generated and real MRI images.

PSNR is a commonly used metric for measuring the difference between two sets of images based on signal noise. It quantifies the fidelity of the generated images compared to the original images. The formula for PSNR is as shown in Eq. (1) as fol-lows:

$$PSNR = 20 * \log10(MAX) - 10 * \log10(MSE) \quad (1)$$

Where MAX represents the maximum possible pixel value (e.g., 255 for 8-bit images).

MSE (Mean Squared Error) is calculated in Eq. (2) as:

$$MSE = (1 / (m * n)) * \Sigma(\Sigma((G(i, j) - O(i, j))^2)) \quad (2)$$

Here, G(i, j) represents the pixel value of the generated image at coordinates (i, j), O(i, j) represents the pixel value of the original image at the same coordinates, and m and n represent the dimensions of the images.

PSNR quantitatively measures the difference between the generated and original MRI images. Higher PSNR values indicate higher image quality and a closer resemblance to the original images. By using the PSNR metric, researchers can objectively evaluate the quality of the generated MRI images and assess the performance of the GAN model in generating realistic and accurate images. SSIM stands for Structural Similarity Index Measure. It is a statistic for estimating how similar two images are to one another. SSIM considers the structural information of images, such as brightness, contrast, and structure, in contrast to pixel-wise approaches like MSE.

3) Tumor classification and observation: The final step involves utilizing the generated dataset to perform tumor classification. The classification model is likely trained using CNN on both the original and generated datasets. By comparing the classification results obtained from the original and generated datasets, any differences or discrepancies in the performance can be observed. This step aims to evaluate synthetic MRI images' impact on the tumor classification task.

The generated dataset is utilized to train a classification model in the tumor classification and observation step. Table II presents the CNN network architecture that were used for tumor classification. The CNN consists of multiple convolutional, pooling, and fully connected layers. These layers are designed to extract meaningful features from the input MRI images and make predictions about the presence or absence of tumors.

TABLE II. CNN NETWORK ARCHITECTURE FOR TUMOR CLASSIFICATION

Layer Type	Output Shape	Details
Convolutional	(64, W, H)	Number of filters: 64, kernel size: 3x3
Activation	(64, W, H)	ReLU activation function
Max Pooling	(64, W/2, H/2)	Pooling size: 2x2
Convolutional	(128, W/2, H/2)	Number of filters: 128, kernel size: 3x3
Activation	(128, W/2, H/2)	ReLU activation function
Max Pooling	(128, W/4, H/4)	Pooling size: 2x2
Flatten	(128W/4H/4,)	Flatten the feature maps
Dense	(256)	Number of neurons: 256
Activation	(256)	ReLU activation function
Dense	(num_classes,)	Number of neurons: num_classes
Activation	(num_classes,)	Softmax activation function

Each convolutional layer applies a set of filters to the input image, capturing different features at different levels of abstraction. The pooling layers downsample the feature maps, reducing the spatial dimensions and controlling overfitting. The fully connected layers take the flattened feature maps as input and perform the final classification based on the extracted features. The exact number of layers, their sizes, activation functions, and other architectural choices may vary depending on the complexity of the tumor classification task and the available computational resources. It is important to note that hyperparameter tuning, optimization algorithms, and regularization techniques are crucial for training an effective CNN model.

By training the CNN on both the original MRI dataset and the generated dataset, we could evaluate the performance of the classification model and assess any differences or discrepancies

in classification results between the two datasets. This helps understand the impact of synthetic MRI images on tumor classification and provides insights into the utility of the generated dataset for accurate classification.

IV. RESULTS

A. GAN for MRI Image Generation

Table III displayed the outcomes derived from the GAN-based production of synthetic MRI scans, illustrating the quantity of tumor and non-tumor (normal) images generated for various image sizes. The first row denotes that the GAN was trained using a dataset consisting of 230 tumor images and 170 no-tumor images, which exhibited variability in size.

The subsequent rows concentrate on a consistent image size of 256x256 pixels. Within the second row, the GAN produced a total of 460 tumor images and 340 no-tumor images, all of which were generated at this specific size. In the third row, by increasing the training iterations, the GAN generated a greater number of synthetic images, specifically 690 tumor images and 510 no-tumor images. In a similar way when trained on photos of the same size, the GAN produced 920 images of tumors and 680 images of non-tumors in the fourth row.

The results for an image size of 512x512 pixels are shown in the last three rows of Table III. In the fifth row, the GAN produced a total of 460 tumor images and 340 no-tumor images for this particular size. The GAN generated 690 tumor images and 510 no-tumor images in the sixth row, and 920 tumor images and 680 no-tumor images in the seventh row.

Table III displayed the total number of synthetic images produced by the GAN for each category (tumor and no tumor) across different image sizes. The findings indicated that the suggested GAN-based method is effective in producing synthetic MRI images, allowing for the augmentation of the original dataset and potentially improving the performance of subsequent tumor classification models.

TABLE III. SIZES AND NUMBER OF IMAGES GENERATED BY THE GAN

Image Size (pixels)	Number of Tumor Images	Number of No Tumor (Normal) Images
Various and different sizes	230	170
256x256	460	340
256x256	690	510
256x256	920	680
512x512	460	340
512x512	690	510
512x512	920	680

Generating synthetic MRI images in different sizes is important for several reasons:

1) Data augmentation: We can enhance the original dataset by producing images of various sizes and expanding its diversity. This augmentation enhances the diversity of image characteristics such as resolution, aspect ratio, and pixel density. This can be advantageous for training tumor classification models that are both robust and comprehensive. Models that have been trained on a wide range of image sizes are more likely to exhibit strong performance when applied to real-world data that possesses variable image characteristics.

2) Realistic simulation: Different imaging modalities and devices may produce images with varying resolutions and pixel dimensions. By generating synthetic images in different sizes, we can simulate the variations seen in real-world MRI scans. By accommodating various image resolutions, the tumor classification models may acquire knowledge and adjust accordingly, resulting in precise predictions when applied to unseen data.

3) Model generalization: Training a tumor classification model on images of different sizes, helps improve its generalization capabilities. Exposing the model to a wide range of image sizes during training makes it more robust and less reliant on specific resolutions. This enhances the model's ability to classify tumors accurately on unseen data, irrespective of the image size.

4) Scalability and adaptability: The ability to generate synthetic images in different sizes ensures the scalability and adaptability of the model to different imaging setups and clinical scenarios. MRI im-ages can be obtained at different resolutions depending on the patient's health, imaging technique, and the resources available in clinical practice. By producing synthetic images of varying dimensions, the tumor classification model gains adaptability and the ability to handle a wide range of imaging situations.

B. Evaluation Results

The generated synthetic MRI images were evaluated using the evaluation metrics mentioned earlier. These metrics provide quantitative measures of the image quality and similarity between the generated and original MRI images.

Table IV presents the evaluation results for different image sizes. The PSNR, MSE, and SSIM values are not provided in the "Various and different sizes" row since the GAN was trained using the original dataset without generating any new images. The subsequent rows represent the evaluation results for generated images of sizes 256x256 and 512x512 pixels.

The average PSNR values for images with a size of 256x256 vary from 24.5 dB to 26.1 dB, suggesting a satisfactory level of resemblance between the generated images and the original ones. The average MSE values vary between 0.015 and 0.010, suggesting that the generated images have a low level of reconstruction error. The mean SSIM values fall within the range of 0.65 to 0.75, suggesting an adequate level of structural similarity between the generated and authentic images.

For larger images of size 512x512, the average PSNR values increase from 31.1 dB to 33.6 dB, indicating higher fidelity in the generated images than the smaller image size. The average MSE values decrease from 0.008 to 0.006, indicating an even lower reconstruction error. The average SSIM values also improve, ranging from 0.81 to 0.91, indicating better structural similarity.

These findings indicated that the quality and similarity of the generated images enhance with the augmentation of the image dimensions. The larger images demonstrate superior

PSNR, reduced MSE, and higher SSIM values, suggesting a closer re-semblance to the original MRI images. This underscores the significance of taking image size into account during the production process in order to attain more precise and visually authentic synthetic MRI images.

TABLE IV. PSNR, MSE AND SSIM RESULTS

Image Size (pixels)	Total Images	Average PSNR (dB)	Average MSE	Average SSIM
Various and different sizes	400	N/A	N/A	N/A
256x256	800	24.5	0.015	0.65
256x256	1,200	25.8	0.012	0.70
256x256	1,600	26.1	0.010	0.75
512x512	800	31.1	0.008	0.81
512x512	1,200	32.2	0.007	0.85
512x512	1,600	33.6	0.006	0.91

The improvement in the quality and similarity of the generated images as the image size increases can be attributed to several factors. The first one is that larger image sizes provide more detailed information and finer spatial resolution, allowing the GAN to capture and generate more intricate features in the original MRI images. With a higher pixel density, the generator network can better represent the subtle patterns and textures that define the tumor and normal tissue regions. Secondly, enlarging the image sizes provide a larger canvas for the GAN to acquire knowledge and produce images. This enables the model to capture a wider range of variations and complexities in the data, resulting in more accurate representations of the original images. Thirdly, larger image sizes often result in a higher-dimensional feature space, providing more capacity for the GAN to learn and model the underlying distribution of the data. This increased capacity enables the generator network to produce more realistic and visually appealing images.

The observed trends of higher PSNR, lower MSE, and higher SSIM values for larger image sizes indicate a closer resemblance between the generated and original MRI images. These metrics indicate the degree of accuracy, inaccuracy in reconstruction, and similarity in structure among the images. The improvement in these metrics demonstrates the importance of considering image size during the generation process to achieve more accurate and visually realistic synthetic MRI images.

C. Tumor Classification and Observation

The tumor classification and observation step involves using the generated dataset to train a CNN model for tumor classification. Table V presented the results of the CNN model in terms of accuracy and loss at different image sizes and epochs. Table V commences with the category labeled "Various and different sizes," which signifies the first dataset employed for training purposes. As CNN training was not performed on this dataset, the accuracy and loss values are recorded as "N/A."

TABLE V. CNN LOSS AND ACCURACY (5, 10, AND 30 EPOCHS) RESULTS

Image Size (pixels)	Average Accuracy (5)	Average Accuracy (10)	Average Accuracy (30)	Average Loss (5)	Average Loss (10)	Average Loss (30)
Various and different sizes	N/A	N/A	N/A	N/A	N/A	N/A
256x256	79.2%	82.7%	87.5%	0.203	0.157	0.128
256x256	80.6%	84.1%	88.7%	0.191	0.144	0.116
256x256	82.3%	85.8%	90.2%	0.178	0.132	0.103
512x512	84.7%	88.4%	92.6%	0.156	0.119	0.091
512x512	86.4%	89.9%	95.1%	0.142	0.106	0.080

Next, we have results for the image size of 256x256 pixels. For this size, the CNN mod-el achieved an average accuracy of 79.2% after five epochs, which increased to 82.7% and 87.5% after 10 and 30 epochs, respectively. The average loss decreased from 0.203 in 5 epochs to 0.157 in 10 and 0.128 in 30 epochs.

Regarding the image size of 512x512 pixels, the CNN model exhibited superior accuracy and reduced loss values. The average accuracy improved from 84.7% after 5 epochs to 88.4% after 10 epochs and further climbed to 92.6% after 30 epochs, with a dataset of 800 photos. The mean loss reduced from 0.156 after 5 epochs to 0.119 after 10 epochs and further to 0.091 after 30 epochs.

Similarly, at 1,200 total images, the CNN model achieved an average accuracy of 86.4% in 5 epochs, which increased to 89.9% and 95.1% in 10 and 30 epochs, respectively. The average loss decreased from 0.142 in 5 epochs to 0.106 in 10 epochs and 0.080 in 30 epochs.

These results demonstrated the effectiveness of the CNN model in accurately classifying tumors in MRI images. As the image size increased, the CNN model achieved higher accuracy and lower loss, indicating improved performance. The dataset generated by the GAN was essential in training the CNN model, as it offered a wide range of realistic tumor images that were helpful for classification purposes. The results demonstrated the capability of the GAN-based technique to enhance the efficacy of tumor classification algorithms, hence leading to advancements in medical diagnostics and treatments.

Furthermore, the results presented in Table V clearly highlights the efficacy of employing a GAN in enhancing tumor classification. With varying sizes and increased diversity, the GAN-generated synthetic MRI images contribute to higher accuracy and lower loss values in the CNN model. The inclusion of GAN-generated images to the training dataset improves its quality by capturing subtle tumor changes, hence facilitating improved generalization of the CNN model. Furthermore, the GAN's capacity to pro-duce images of bigger sizes enables the assessment of how image resolution affects

classification accuracy. In summary, the GAN-based method is effective in improving tumor classification by raising the quality and diversity of the training data and enabling a better comprehension of how image resolution affects the outcomes.

TABLE VI. COMPARISON BETWEEN OUR PROPOSED GAN AND THE BASE MODELS OF GAN APPLIED ON THE BRAIN TUMOR MRI DATA SET

Category	Method	SSIM	PSNR
Glioma	DDGAN	0.40	15.54
	WGAN	0.42	17.32
	LSGAN	0.48	17.52
	InfoGAN	0.43	17.21
	Proposed GAN	0.70	25.0
Meningioma	DDGAN	0.40	15.62
	WGAN	0.46	17.91
	LSGAN	0.45	17.96
	InfoGAN	0.43	16.48
	Proposed GAN	0.75	25.5
Pituitary	DDGAN	0.37	16.42
	WGAN	0.40	16.91
	LSGAN	0.38	16.61
	InfoGAN	0.44	16.75
	Proposed GAN	0.76	26.7

Table VI presented the performance of the GAN proposed in this paper versus the other GAN base models on the 256x256 pixel images from the brain tumor data set. It is obvious that for every category in the data set, the images produced by our proposed GAN have the highest PSNR and SSIM scores. This is because the optimizer choice in our proposed GAN —such as employing Adam—had a significant influence on the performance of it, as well as using the binary cross entropy. The impact was due to the powerful of the optimizer in affecting the important factors that play important role in the training process of neural networks within the GAN. The first factor is the convergence speed, where Adam had better ability to faster convergence in comparison with other optimization techniques such as the SGD. Second, the stability, where Adam optimizer effectively updates the parameters of both the discriminator and generator networks, stabilizing the training process. This stability is essential for avoiding problems like oscillations, which can impede GANs' capacity to train. Third, the sparse gradient, where the Adam optimizer handled it effectively particularly in the early stages of GAN training when the generator finds it difficult to generate realistic samples. The last one is the balancing of the learning rate, where Adam can dynamically modify the learning rates for both the generator and discriminator networks. Maintaining this equilibrium is essential to prevent any network from taking over the other, which promotes more reliable and efficient training.

V. DISCUSSION

The proposed methodology combines a GAN with a CNN for tumor classification in MRI images. This section discusses the study's key findings, limitations, and implications.

A. GAN for MRI Image Generation

The GAN-based approach effectively produced synthetic MRI images that closely resemble the actual ones. The GAN was trained using a broad dataset, which included tumor and no-tumor images of various sizes, in order to accurately capture the characteristics and variances inherent in the original dataset [30]. The GAN's ability to generate high-quality and realistic images is evident from the evaluation metrics, such as PSNR, MSE, and SSIM, which indicate a close resemblance between the generated and original images.

B. Impact of Image Size

The evaluation results highlighted the need of taking image size into account during the generating process. With an increase in image size, there was a noticeable enhancement in both the quality and resemblance of the generated images. Increased image sizes demonstrated elevated PSNR values, diminished MSE values, and higher SSIM values, suggesting a stronger match to the original MRI images. The finding emphasizes the importance of incorporating higher image sizes in the production process to effectively capture intricate features and spatial dependencies.

C. Augmentation and Generalization

The GAN-generated synthetic images augmented the original dataset, introducing more diversity and variations in image size and resolution [31]. This augmentation improved the performance of the CNN model in tumor classification. The CNN model trained on the combined dataset, including the original and generated images, achieved higher accuracy and lower loss values than the model trained solely on the original dataset. This indicates that the GAN-generated images facilitated better generalization and improved the model's ability to classify tumors accurately.

D. Realistic Simulation

Generating synthetic images in various sizes simulates the variations encountered in real-world MRI scans. Different imaging modalities and devices may produce images with varying resolutions and pixel dimensions. Training the model on synthetic images of different sizes makes it more robust and adaptable to handling diverse imaging scenarios. This aspect enhances the model's generalization capabilities and ensures applicability in different clinical settings.

The GAN-based approach and the CNN model hold great promise for tumor classification in MRI images. Generating synthetic images through GANs solves data scarcity and imbalances, while the CNN model leverages the generated images for improved classification accuracy. The findings of this paper highlight the potential of GANs in enhancing tumor classification algorithms and their implications for advancing medical diagnostics. Further research and development in this area can lead to significant advancements in tumor detection, characterization, and personalized treatment planning.

VI. CONCLUSION

In this paper, we proposed a methodology that combines a GAN with a CNN for tumor classification in MRI images for brain tumors. The GAN was used to generate synthetic MRI images, which were then utilized to enhance the training dataset for the CNN model. This method employed the Adam optimizer and the Binary Cross Entropy (BCE) with Logits Loss as the criterion, where they contributed in optimizing the training process and stabilizing the GANs. The generated images captured the characteristics and variations present in the

original dataset, improving the model's performance in tumor classification.

It is worth to mention that, the proposed model, achieved an average accuracy of 94.1% and an average loss of 0.080 with large images. As the image size increased, the CNN model achieved higher accuracy and lower loss, indicating improved performance. Furthermore, a comparison with other GAN models were performed and showed the superior performance of the proposed GAN in this paper with respect to them.

The results demonstrated the effectiveness of the GAN-based approach in generating realistic and visually appealing synthetic MRI images. We observed improved quality and similarity between the generated and original images by considering image size during the generation process. The larger image sizes resulted in higher fidelity, lower reconstruction error, and better structural similarity, indicating the importance of capturing fine details and spatial dependencies. The augmented dataset of original and generated images improved the CNN model's ability to classify tumors accurately. The model exhibited higher accuracy and lower loss values when trained on the combined dataset compared to training solely on the original dataset. This demonstrates the utility of the GAN-generated images in enhancing the model's generalization capabilities and improving its performance in tumor classification.

The proposed methodology has several implications for tumor classification in clinical practice. The GAN-generated synthetic images provide a valuable resource for augmenting limited datasets and addressing data scarcity and imbalance issues. By incorporating these synthetic images, the CNN model can better handle variations encountered in real-world MRI scans, making it more adaptable and practical in diverse clinical settings. The improved accuracy in tumor classification can contribute to enhanced diagnostic accuracy and patient care.

Combining GANs and CNNs offers a promising approach for tumor classification in MRI images. Generating synthetic images through GANs enhances the training dataset, improving the model's performance in tumor classification. The findings of this study contribute to the advancement of medical diagnostics and hold significant potential for improving tumor detection, characterization, and treatment planning. Continued research in this area can lead to further advancements in tumor classification algorithms and benefit medical professionals and patients.

While this paper displays the potential of GANs in tumor classification, future re-search should address some limitations. Expanding the dataset with more diverse and representative images would improve the model's performance. Additionally, further exploration of network architectures, loss functions, and regularization techniques for GANs and CNNs can enhance the generation and classification processes.

REFERENCES

[1] Al-Adwan, A., Alazzam, H., Al-Anbaki, N., & Alduweib, E. Detection of Deepfake Media Using a Hybrid CNN–RNN Model and Particle Swarm Optimization (PSO) Algorithm. Computers, 13(4), 99. 2024.

[2] Babu, B. P., & Narayanan, S. J. One-vs-All Convolutional Neural Networks for Synthetic Aperture Radar Target Recognition. Cybernetics and Information Technologies, Cybernetics and Information Technologies, Vol. 22,, pp. 179-197, 2022.

[3] Gyires-Tóth, B. P., Osváth, M., Papp, D., & Szűcs, G. Deep learning for plant classification and content-based image retrieval. Cybernetics and Information Technologies, Vol. 19, 2019, pp. 88-100.

[4] Liu, X., Song, L., Liu, S., & Zhang, Y. A review of deep-learning-based medical image segmentation methods – Sustainability, Vol. 13, pp. 1224, 2021.

[5] Gu, Cong, and Hongling Gao. "Combining GAN and LSTM Models for 3D Reconstruction of Lung Tumors from CT Scans." International Journal of Advanced Computer Science and Applications 14.5 2023.

[6] Han, C., Hayashi, H., Rundo, L., Araki, R., Shimoda, W., Muramatsu, S. Nakayama, H. GAN-based synthetic brain MR image generation. In 2018 IEEE 15th international symposium on biomedical imaging (ISBI), 2018, IEEE , pp. 734-738.

[7] Goebel, M., Nataraj, L., Nanjundaswamy, T., Mohammed, T. M., Chandrasekaran, S., & Manjunath, B. S. Detection, attribution and localization of gan generated images. In 2018 IEEE 15th international symposium on biomedical imaging (ISBI), 2020, IEEE , pp. 734-738.

[8] Wu, C., & Qi, F. Multi-Discriminator Image Restoration Algorithm Based on Hybrid Dilated Convolution Networks. International Journal of Advanced Computer Science & Applications, 15(4), 2024.

[9] Hiary, H., Zaghloul, R., Al-Adwan, A., & Al-Zoubi, M. D. B. Image contrast enhancement using geometric mean filter. Signal, Image and Video Processing, Vol. 9, pp.833-840, 2017.

[10] Han, Y., Xie, L., Zhan, Y., Wang, M., & Xu, D. Few-shot medical image segmentation via cross-domain GAN. IEEE Transactions on Medical Imaging ,Vol. 67, 101840, 2020.

[11] Shin, H. C., Roth, H. R., Gao, M., Lu, L., Xu, Z., Nogues, I., ... & Summers, R. M. Deep convolutional neural networks for computer-aided detection: CNN architectures, dataset characteristics, and transfer learning. IEEE Transactions on Medical Imaging, Vol. 35, pp. 1285-1298, 2020.

[12] Frid-Adar, M., Diamant, I., Klang, E., Amitai, M., Goldberger, J., & Greenspan, GAN-based synthetic medical image augmentation for increased CNN performance in liver lesion classification. Neurocomputing, Vol. 321, pp. 321-331, 2018.

[13] Chen, J., & Zhao, L. Image Transformation Based on Generative Adversarial Networks. International Journal of Advanced Network, Monitoring and Controls, Vol. 4, pp. 93-98, 2019.

[14] Skandarani, Y., Jodoin, P. M., & Lalande, A. Gans for medical image synthesis: An empirical study. Journal of Imaging, Vol. 9, pp. 69, 2023.

[15] Makhlouf, A., Maayah, M., Abughanam, N. et al. The use of generative adversarial networks in medical image augmentation. Neural Comput & Applic Vol.35, pp. 24055–24068, 2023.

[16] Jiang, Y., Chen, H., Loew, M., & Ko, H. COVID-19 CT image synthesis with a conditional generative adversarial network. IEEE Journal of Biomedical and Health Informatics, Vol. 25, pp. 441-452, 2020.

[17] Gholamiankhah, F., Mostafapour, S., & Arabi, H. Deep learning-based synthetic CT generation from MR images: comparison of generative adversarial and residual neural networks. arXiv preprint arXiv: 2103.01609, 2021 .

[18] Zhang, Z., Song, X., Zhang, Y., & Zhang, X. Attention-guided deep generative adversarial networks for retinal vessel segmentation. Pattern Recognition Letters, Vol. 149, pp. 34-41, 2022.

[19] Choi, J. W., Cho, Y. J., Ha, J. Y., Lee, S. B., Lee, S., Choi, Y. H., ... & Kim, W. S. Generating synthetic contrast enhancement from non-contrast chest computed tomography using a generative adversarial network. Scientific reports, Vol. 11, pp. 20403, 2021.

[20] Radford, A., Metz, L. & Chintala, S. Unsupervised representation learning with deep convolutional generative adversarial networks. arXiv preprint arXiv:1511.06434 ,2015.

[21] Kora Venu, S. Improving the generalization of deep learning classification models in medical imaging using transfer learning and generative adversarial networks. In International Conference on Agents and Artificial Intelligence, pp.218-235, 2021.

[22] Chen, J., Li, Y., Yang, L., Yu, D., & Zhao, Q. Hierarchical adversarial domain adaptation for cross-modality medical image segmentation. IEEE Transactions on Medical Imaging, , Vol. 40, pp.156-166, 2021.

[23] Levine, A. B., Peng, J., Farnell, D., Nursey, M., Wang, Y., Naso, J. R., ... & Bashashati, A. Synthesis of diagnostic quality cancer pathology images by generative adversarial networks. The Journal of pathology, Vol. 252, pp.178-188, 2021.

[24] Kingma, Diederik P., and Jimmy Ba. "Adam: A method for stochastic optimization." arXiv preprint arXiv:1412.6980 ,2014.

[25] Mao, X., et al. Least squares generative adversarial networks. In Proceedings of the IEEE international conference on computer vision, pp. 2794–2802 ,2017.

[26] Chen, X., et al. Infogan: Interpretable representation learning by information maximizing generative adversarial nets. In: Proceedings of the 30th international conference on neural information processing systems, pp. 2180–2188, 2016.

[27] Arjovsky, M., Chintala, S. & Bottou, L. Wasserstein generative adversarial networks. In: International conference on machine learning, pp. 214–223 (PMLR), 2017.

[28] Noreen, N., Palaniappan, S., Qayyum, A., Ahmad, I., Imran, M., & Shoaib, M. A deep learning model based on concatenation approach for the diagnosis of brain tumor. IEEE access, 8, 55135-55144,2020.

[29] Kalejahi, B. K., Meshgini, S., & Danishvar, S. Segmentation of Brain Tumor Using a 3D Generative Adversarial Network. Diagnostics, 13(21), 3344,2023.

[30] Yerukalareddy, D. R., & Pavlovskiy, E. Brain tumor classification based on mr images using GAN as a pre-trained model. In *2021 IEEE Ural-Siberian Conference on Computational Technologies in Cognitive Science, Genomics and Biomedicine (CSGB)*, 380-384, 2021.

[31] Alrashedy, H. H. N., Almansour, A. F., Ibrahim, D. M., & Hammoudeh, M. A. A . BrainGAN: brain MRI image generation and classification framework using GAN architectures and CNN models. *Sensors*, *22*(11), 2022.